ELSEVIER

Contents lists available at ScienceDirect

International Journal of Electrical Power and Energy Systems

journal homepage: www.elsevier.com/locate/ijepes



Robust dispatch for electrical–thermal combined smart building considering impacts of uncertainties on thermal side

Weijie He^a, Fanrong Wei^{a,*}, Xiangning Lin^a, Samir M. Dawoud^b

- ^a State Key Laboratory of Advanced Electromagnetic Engineering and Technology, Huazhong University of Science and Technology, Wuhan, Hubei 430074, China
- b Department of Electrical Power and Machines Engineering, Faculty of Engineering, Tanta University, Tanta, Egypt



Keywords:
Smart building
Electrical-thermal integrated
Robust dispatch
Uncertain factor
Thermodynamic model
Co-optimization framework

ABSTRACT

The close connection between electrical energy and thermal energy is an important attribute of current smart buildings. Most previous works aim to emphasize the important role of the power side, thus neglecting the accuracy of the thermal side model. At the same time, from the perspective of the building layer, uncertainties such as random solar radiation will affect not only the electrical side but also the thermal side. This paper presents a robust day-ahead dispatch for the smart building which is integrated with coupled electrical system and thermal system. First, we propose a comprehensive thermodynamic model to evaluate impacts of uncertain factors on the thermal system of the smart building in this paper. Subsequently, a robust co-optimization framework is formulated to cope with the uncertainties in a unified manner. To deal with the nonlinearity brought by the electrical-thermal coupled relationship, we propose a piecewise linearization method to convert the nonlinear robust co-optimization dispatch to a linear min-max-min problem, which can be solved by a traditional decomposition algorithm. Case studies demonstrate that the impact of solar radiation uncertainty on the thermal side accounts for 16.2% of that on the power side, indicating its significance. Compared with traditional thermodynamic models, the refined model can better reflect the actual working conditions of the building thermal storage system. The robust scheduling model proposed in this paper that considers the uncertainty on both sides jointly improves the conservatism of traditional scheduling schemes while achieving better economic benefits.

1. Introduction

As one of the most important energy consumers in the city, buildings account for a significant portion of total energy consumption. With the proposal of the green building concept, coordinating and scheduling the energy consumption of various buildings is an important measure to reduce energy consumption and build a energy resource guarantee system for the society [1].

As the nation pays increasing attention to the energy crisis and environmental demands, the integration of distributed photovoltaic (PV) systems with buildings has become tighter, initially forming a prototype of an integrated power generation and consumption unit [2]. However, with the rising penetration rate of renewable energy generation, PV systems are often restricted from connecting to the grid due to reasons such as reducing power quality and threatening the safety of microgrids, leading to actual losses of unused solar energy. At the same time, the grid connection of PV generation, characterized by its randomness and volatility, may burden the real-time power balance and safe, stable operation of the grid. Against this backdrop, building operators need to

design more tailored and refined autonomous scheduling strategies to better match the energy demands of buildings.

The traditional power scheduling field has proposed various optimized scheduling strategies, providing a certain basis for research on the above issues. However, traditional power scheduling mainly targets the power grid, optimizing its economic operation by adjusting the operational status of power plants and transmission lines. Clearly, the existing electrical grid scheduling strategies cannot be directly applied to solve the economic and safety issues brought about by the integration of photovoltaic systems with buildings. Installing energy storage systems at user terminals may be a feasible solution. Ref. [3] suggests that integrating battery storage into residential systems with wind and solar power is beneficial for implementing an energy system that balances efficiency and space constraints, achieving optimal energy management for the building. Ref. [4] analyzes the economic aspects of building integrated photovoltaic to emphasize the role of battery storage in the form of saving electricity costs, and the economic benefits of carbon reduction. The above research has solved

E-mail address: M202372468@hust.edu.cn (F. Wei).

^{*} Corresponding author.

Nomenclature								
Sets and Indices								
i	internal surface	0	external surface					
Acronyms		-						
PV	photovoltaic	SOC	state of charge					
TES	thermal energy storage	SO	stochastic optimization					
HP	heat pumps	RO	robust optimization					
TSM	thermal storage material		•					
Parameters and Variables								
g_t	solar radiation	T_{am}^t	ambient temperature					
T_{n}^{t}	temperature of TSM	m_t	circulation air					
T_{R}^{t}	room temperature	T_{ag}^t	air gap temperature					
T_{p}^{t} T_{k}^{t} T_{k}^{t} T_{k}^{t} T_{i}^{t} T_{i}^{t} T_{i}^{t} T_{i}^{t} T_{i}^{t}	surface temperature	h_o^{as}, h_i	convective coefficients					
h_i^r, h_o^r	radiative coefficients	A_o, A_i	air contact areas					
T_o^t, T_i^t	node temperature	C_A	specific heat capacity of air					
$Q_{l_{Pak}}^{t}$	total amount of heat leakage	Q_{o-a}^t , Q_{i-a}^t	heat leaked by conduction					
$Q_{leak}^t \ Q_{o-p}^{rt}, Q_{i-p}^{rt}$	heat leaked by radiation	Q_{ctrl}^t	controllable heat transmission					
P_{TL}^t	thermal load	Q_{a-p}^t	thermal flow from the air gap to TSM					
Q_o^t	thermal loss	Q_{am-o}^{t}	thermal flow from the environment					
$Q^{t}_{\Delta ext{-}o},~Q^{t}_{\Delta ext{-}i}$	enthalpy increment	Q_{j-i}^{rt}	energy flow					
Q_{am-k}^{rt}	thermal flow from the environment to	Q_{k-R}^t , Q_{k-j}^t	thermal flow from envelop k to the room space and envelop j					
ит-к	envelop j	K-K K-j						
C_p	specific heat capacity	T_p	specific heat capacity					
$C_p \ T_p^{\min}, T_p^{\max}$	lower and upper boundaries of temperature	α , β , γ	the fitting parameters of the melting curve					
	in phase change process							
m_p	mass of TSM	H	enthalpy difference of TSM					
S	SOC of TESS	p_{db}^t, p_{ds}^t	day-ahead purchase and day-ahead sell price					
P_{rb}^{t}, P_{rs}^{t} P_{rb}^{t}, P_{rs}^{t} P_{PV}^{t} P_{L}^{t} E_{ce}^{t}	real-time purchase and sell price	$\frac{P_{db}^t}{\bar{\theta}}, \ P_{ds}^t$	day-ahead purchase and sell power					
P_{rb}^t , P_{rs}^t	real-time purchase and sell power		second-stage optimal economic dispatch cost					
P_{PV}^{t}	power of PV	E_c^t P_{HP}^t E_{ct}^t	total energy absorbed					
P_L^t	power of loads	P_{HP}^{t}	power of HP					
E_{ce}^{t}	electrical energy produced	E_{ct}^{r}	thermal energy released					
$\eta_e^i, \eta_0, \beta, \alpha_c$	coefficients of PV thermal process	E_T^{ι}	solar energy absorbed by the back-sheet of PV cell					
h_{PV},A_{PV}	convective coefficient and the contact area	μ_t , μ_0	real-time coefficient of performance and ideal COP of HP					
	between the back-sheet and the front of PV							
~ + -	panel	A+ A-	1 1 11 1 1					
$\tilde{g}_t, g_t^+, g_t^-$	predicted nominal value, upward bias and	\hat{g}_t^+,\hat{g}_t^-	upper bound and lower bound					
z_{t}^{+}, z_{t}^{-}	downward bias of the solar radiation	Γ	hudget of uncontainty					
z_t , z_t	mutually exclusive variables	1	budget of uncertainty					

the problem of electrical energy management in buildings, but it has also ignored two core issues. First, given the limited availability of large-capacity, long-duration energy storage methods that are economically viable for microgrids, most of which have issues with short lifespan and high costs, and are constrained by geographical conditions and efficiency factors, battery storage systems are not suitable for use in the microgrids. Second, increasing interactions between the electrical and thermal systems in buildings have the potential to transform the independent energy systems into smart buildings [5]. In this development context, the co-management of electrical and thermal energy flows in buildings is a key issue that requires attention [6]. To fully leverage the energy-saving advantages of photovoltaic-integrated buildings [7], there is an urgent need to find an economical and environmentally friendly storage method that is compatible with it, and to study its reasonable scheduling strategies. Compared with battery storage, converting electrical energy into heat/cold energy for storage has the advantages of larger storage capacity and lower economic cost, and can also establish a close connection between the two energy flows. By combining multiple materials and designing the phase change temperature point of the thermal energy storage material near the comfortable temperature of the human body, air-conditioning-level cold and heat storage functions can be achieved. Moreover, integrating with the building on the energy consumption side can solve the

problem of loss in the transportation process. In this structure, unifying and centrally managing originally independent energy units within a building (including distributed photovoltaics, thermal energy storage systems(TES), heat pumps and related technologies) is a very important attribute of smart buildings [8]. Ref. [9] proposes an optimal scheduling method for the interaction between smart buildings and distribution networks based on the thermal storage characteristics of buildings, contributing to the operating costs reduction of the smart buildings. Ref. [10] proposes a novel flexible energy building concept, based on smart control, high density latent heat storage and smart grids, able to simultaneously allow end-users to save 20% on electricity bills and reduce carbon emissions. Ref. [11] proposes to use thermal storage combined with solar energy to save energy and provide heating in distributed buildings. Under this kind of combined energy scheduling framework, the thermal demand can be fulfilled by the clean electric energy with heat pumps (HP) or electric heaters from the building itself or the microgrids. Meanwhile, the integration of thermal energy storage endows the thermal system with the ability to alter the heating/cooling load profile and respond to the day-ahead and real-time power regulation demands from the electrical side. Therefore, the combination of multiple energy systems in smart building creates new opportunities for enhancing efficiency, flexibility, and reducing operating costs.

There exist extensive studies on the electrical-thermal combined system. Ref. [12] introduces a fully hybrid renewable energy system,

including wind turbines, PV and thermal storage units, which realizes clean energy supply on both the electric and thermal sides, but the modeling of the thermal side is too simple. Ref. [13] proposes a new energy management system model for isolated microgrids, integrating thermal energy resources such as heat pumps and thermal storage systems, while considering thermal loads. Although more thermal resources are considered, a complete thermal network model is not established. Ref. [14] utilizes thermal energy storage systems to store energy during off-peak hours and discharge it at high load demand, minimizing the building's electricity consumption during peak hours, completely ignoring the building's heat demand. Ref. [15] proposes a design management and optimization framework of photovoltaic heat pump system integrating thermal energy storage and battery energy storage based on a nearly zero-energy building in cold region, but does not reflect the impact of the thermal side. Ref. [16] proposes an optimization strategy for wind/PV/thermal power integration system. Nevertheless, the dispatch strategies mentioned above are mainly concerned with the details in electrical systems, while the thermal systems are simplified as controllable loads or energy storage devices, not yet considering the thermal constraints faced in practice. Note that there are indeed some studies which have paid more attention to the actual thermal transfer process. Refs. [17,18] propose general TES models which take detailed heat transfer analysis into account, while the seasonal and daily heat demand for thermal energy storage are taken into consideration in Ref. [19]. However, these models could still be extended further to analyze the thermal system and electrical system in a more comprehensive way. For instance, the state of charge (SOC) of TES in the literature above is only assigned to be an index to avoid overcharge or depletion risks, not related to any thermal side variable, thus the coupled impacts of charging actions on the performance of thermal side are neglected.

In addition to the accurate and detailed modeling of the electricalthermal combined system, the impact of external uncertainties also deserves deep consideration. Ref. [20] considers the operational uncertainties encountered in real-time operations due to renewable energy sources and electrical loads in the proposed building energy management system. Ref. [21] considers the influence of SOC measurement uncertainty on the power side in an electric heating system . Ref. [22] specifically analyzes the heat demand response when power supply is interrupted due to uncertain extreme events. Ref. [23] considers the uncertainty of ambient temperature in a coordinated operation of an integrated electricity and heating system and converts it into uncertain parameters on the electricity side. Ref. [24] proposes an adaptive robust day-ahead energy-reserve co-optimization approach for urban energy systems. However, in the above work, the impacts of uncertainties are only within the electrical side, while the thermal side is assume to be fully controllable and be immune against uncertainties. Actually the researches on building thermodynamics verify that the environmental factors have significant impacts on the performances of thermal system side. For instance, Ref. [25] analyzes the thermal behavior of curved roof buildings exposed to solar radiation and wind flow, indicating that the larger of the building envelop exposed to the ambient environment, the more significant the impacts of environmental uncertainties on the thermal loads. In addition, Ref. [26] investigates the effect of solar radiation models on the determination of energy performance with the hourly meteorological data in Turkey and concludes that the average deviation is up to 12.5% for space cooling load intensity. Refs. [27,28] demonstrate that the sensitivity of heat consumption corresponds to solar radiation. It can be seen that the scheduling scheme is likely to be infeasible when applying to the thermal side, when the actual values of the environmental variables deviate from forecast ones. The above indicates that uncertainty factors, represented by environmental variables such as solar radiation, can have a significant impact on the generation of renewable energy and the process of thermal transmission within smart buildings. At the same time, due to environmental variability, this impact cannot be ignored.

When considering uncertainty factors, the optimization solution algorithms will become more complex. For scenarios where uncertain distributions are known, stochastic optimization (SO) approaches are generally used [29,30], while robust optimization (RO) is widely adopted merely with the boundaries of uncertain distribution [31,32]. Refs. [33,34] propose unified stochastic and robust unit commitment models that take advantage of both SO and RO approaches. Ref. [35] uses a RO with adjustable uncertainty budget dispatch model for hybrid wind/ photovoltaic (PV)/ hydro/ thermal energy system to make coordination between reliability and economy. For small microgrids such as buildings, robust scheduling is more flexible and has more practical engineering significance.

In general, existing studies on smart building energy systems generally have problems such as oversimplification of the thermal side model, separation of the electric and thermal systems, neglect of thermal side uncertainties, and weak scheduling flexibility. In response to the above problems, this paper first proposes a smart building thermal model that considers a more sophisticated thermal network based on the Ref. [17]. Then, the influence of uncertainty factors on both sides of the electric and thermal systems is analyzed by establishing an electric-thermal robust collaborative optimization scheduling model. A piecewise linearization method is proposed to transform the nonlinear two-stage problem into linear main and sub-problems, and iteratively solve it in combination with the strong duality theory. Uncertainty adjustment parameters are added to the model, allowing dispatchers to flexibly select the conservativeness of the scheduling strategy according to user needs. Finally, the case analysis verifies the necessity of considering the uncertainty factors of the thermal system and the advantages of the electric-thermal robust collaborative optimization scheduling model. To highlight the uniqueness of this method, Table 1 compares the proposed method with existing references. The contributions can be summarized as follows.

- (1) A fine thermodynamic model of the smart building is established based on the thermal network method. Compared with the models integrated in previous dispatch frameworks, the proposed one can reflect the thermal side impacts of environmental variables and their uncertainties.
- (2) The electrical-thermal conversion equations are formulated to couple the multi-energy systems in the smart building as a unified one. With the conversion equations, the SOC in the electrical side is transformed into thermal variables. Thus the correlation between the electrical side charging/discharging profile and the thermal-side performance has been established.
- (3) A novel robust dispatch considering the room temperature comfort zone for smart building is proposed. With the unified analysis of uncertainties, the comprehensive worst case can be found, while the unlike-to-happen scenarios can be avoided, further enhancing the reliability and economy performances of the scheduling scheme.
- (4) A new linearization method with additional reliability constraint is proposed to transforms the nonlinear robust dispatch into a linear problem, which can be solved based on the strong duality theory and the decomposition approach.

The rest of the paper is organized as follows: Section 2 presents a typical thermodynamic model of smart building. Section 3 proposes a novel robust dispatch strategy for the electrical-thermal combined system. Section 4 develops a decomposition algorithm. Simulation results and the conclusion are provided in Section 5 and Section 6, respectively.

2. Thermodynamic model of smart building

In this section, a detailed thermodynamic model is formulated to analyze the environmental sensitivity of the smart building illustrated in Fig. 1.

Table 1
Comparison of the methods in this paper with existing references.

References	Energy flows		Thermal Model	Electrical– thermal coupling	Uncertainty		Advantages			
	Electricity	Thermal			Electricity	Thermal	Robustness	Economical	Security	Comfort
[3,4]	1							1		
[12]	/	1	Simplified	Uncoupled				✓		
[13]	/	✓	Simplified	Uncoupled				✓		/
[14]	/	✓	Ignored	Uncoupled				✓	✓	
[15,16]	/	✓	Ignored	Uncoupled				✓		
[17,18]	/	✓	Detailed	Uncoupled				✓		
[19]	/	✓	Detailed	Uncoupled		/		✓		/
[20,22]	✓	/	Simplified	Coupled	✓			✓	✓	
[21,23]	/	✓	Simplified	Uncoupled	✓			✓		/
[24]	/	✓	Simplified	Uncoupled	✓		✓	✓		
Proposed	1	✓	Refined	Coupled	✓	✓	✓	✓	1	✓

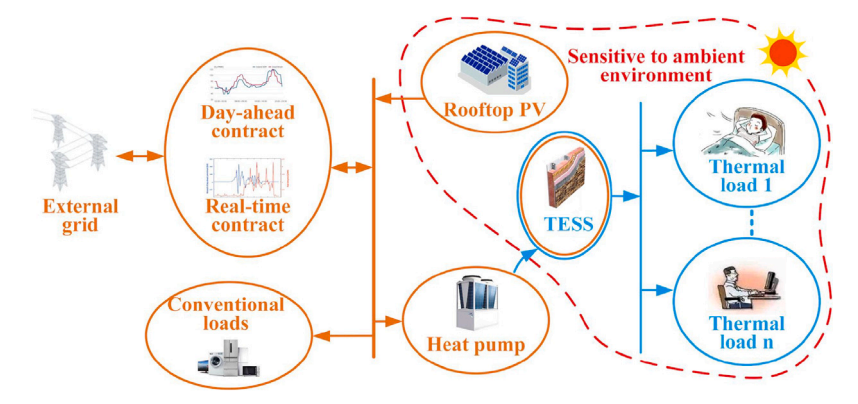


Fig. 1. The energy flow of electrical-thermal combined smart building [15].

The thermodynamic model is formulated based on a thermal system prototype which is proposed in Ref. [36]. As presented in Fig. 2, the encapsulated thermal storage material (TSM) is placed into the residential side building envelop (wallboard). The TSM has a function and structure similar to those of a ground heating. The wallboard is composed of a concrete in outer layer, a polystyrene plate in the secondary layer, a hollow brick layer, and the interior panel as the innermost layer. The hollow bricks are densely paved with polyethylene pipes, in which TSMs are encapsulated to prevent TSM leakage and avoid the corrosion of the wallboard. An air gap is arranged between the polyethylene pipes to increase the air contact area, thereby increasing the heat exchange. In the process of heat storing, heat pump converts the electricity into heat, which is transmitted into encapsulated TSM using the refrigerant medium. Assume that three sides of the building envelops, including the one integrated with TSM, are faced with shade, while the rest is exposed to the solar radiation. Note that the uncontrollable heat exchange process, which is indicated by black lines, includes two forms: one is heat conduction between the parts in direct contact, such as the air gap to external surface of the building envelops, and the other is heat radiation between the parts without direct contact, such as the TSM to the internal surface of the building envelops. Moreover, only relying on heat conduction and radiation may not meet the needs of indoor temperature control. Therefore, inspired by the circulated air flow in a passive solar-powered green building, a forced convection with ventilating fan is used to accelerate the heat exchange in a controllable manner, apart from the natural convection and spontaneous heat radiation between the TSM wallboard and the indoor air, which is presented as blue lines in Fig. 2. The heat leakage, which contributes in part to the thermal balance, is also considered in this thermodynamic model.

In the framework of the above-mentioned smart building, the electric loads of the building are directly supplied by the smart building,

which can be connected to the external grid, and the indoor temperature regulation service is provided by TES. The electric-thermal systems are coupled with inverter HPs. There exist two working modes of TES.

Mode 1: Heat storage mode, where electricity is converted into heat and stored in the TES with a power balance limitation, and the only controllable device is the HP.

Mode 2: Heat release mode, where heat is released into the room with the thermal balance limitation, and the only controllable device is the ventilating fan.

In this model, solar radiation g_t , ambient temperature T^t_{am} and TSM temperature T^t_p serve as the input variables; the mass flow rate of circulation air m_t is the controllable variable; while the room temperature T^t_R , the air gap temperature T^t_{ag} and the surface temperature of the building envelops T^t_k , $k \in N$ are the state/output variables.

According to the law of thermodynamics, the uncontrollable heat leakage of TSM envelop can be expressed by Eqs. (1)–(5). More specifically, (1) denotes the total amount of heat leakage. Eqs. (2)–(3) stand for the heat leaked to the external surface of the building envelops by conduction and radiation, respectively, while (4) and (5) represent the heat leaked to the internal surface by conduction and radiation, respectively.

$$Q_{leak}^{t} = Q_{o-a}^{t} + Q_{o-b}^{rt} + Q_{i-a}^{t} + Q_{i-a}^{rt}$$
(1)

$$Q_{o\text{-}a}^{t} = h_o A_o \left[T_o^t - T_{ag}^t \right] \tag{2}$$

$$Q_{o\cdot p}^{rt} = h_o^r A_o \left[T_o^t - T_p^t \right] \tag{3}$$

$$Q_{i-a}^t = h_i A_i \left[T_i^t - T_{ag}^t \right] \tag{4}$$

$$Q_{i-p}^{rt} = h_i^r A_i \left[T_i^t - T_p^t \right] \tag{5}$$

where h_o , h_i , h_o^r and h_i^r represent the convective and radiative coefficients of TSM with the external surface and internal surface of the wallboard, respectively. A_o and A_i are air contact areas of the external

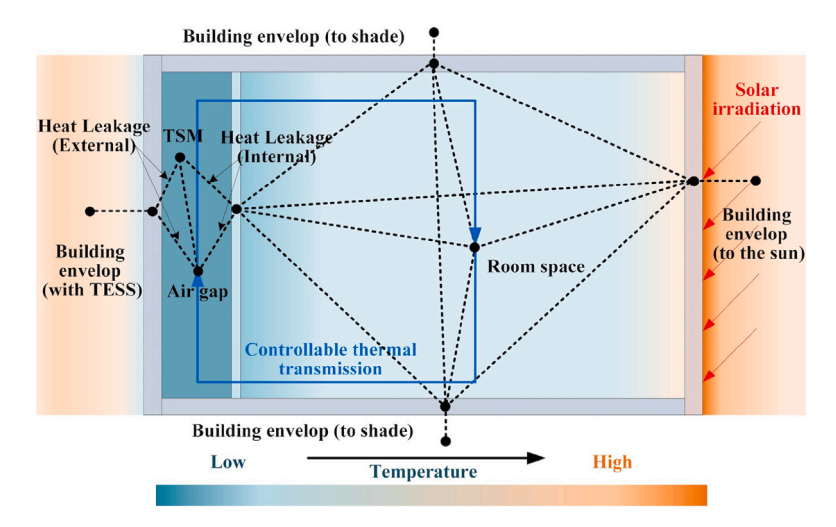


Fig. 2. A typical thermodynamic network for smart building [36].

surface and internal surface, respectively. T_o^t and T_i^t stand for the node temperature of the external surface and internal surface, respectively.

The controllable heat transmission with the forced air circulation is calculated as the enthalpy difference between the inlet and outlet air flows:

$$Q_{ctrl}^{t} = m_t C_A \left[T_R^t - T_p^t \right] \tag{6}$$

where C_A is the specific heat capacity of air, T_R^t is the temperature of room space, and m_t denotes the massive flow rate of circulating air, which is restricted by m^{\max} as

$$0 \le m_t \le m^{\max} \quad \forall t \tag{7}$$

Note that, Eq. (6) contains the bilinear expression of m_t with T_R^t . Therefore, a brief discussion is conducted to replace the expression of Eq. (6):

(1) If $m \neq 0$, an optimized indoor temperature T_R^t should be kept at T_R^{\max} . Otherwise, m can be further decreased to reduce the energy consumption of thermal system.

(2) If
$$m = 0$$
, Q_{ctrl}^t in (6) will be 0 for any T_R^t .

Therefore, the linear Eq. (8) is equivalent to (6) in this optimization problem by replacing variable T_R^t with constant T_R^{\max} .

$$Q_{ctrl}^{t} = m_t C_A \left(T_R^{\text{max}} - T_p^t \right) \tag{8}$$

The thermal load P_{TL}^t can be defined as the total energy transferred in controllable and uncontrollable ways.

$$P_{TL}^t = Q_{ctrl}^t + Q_{leak}^t (9)$$

The thermal energy balance equations are formulated as (10)-(18). In particular, Eq. (10) denotes the TSM heat balance equation. The heat exchange between TSM and the air gap is equal to the one between the air gap and surfaces of the storage envelop and the room space. Eqs. (11)-(12) represent the heat balance equations of the TSM wall exterior. The heat flow from the external environment to the TSM wall exterior is equal to the heat exchange between the TSM wall exterior and the air gap, TSM and other building walls. What is more, Eq. (13) indicates that the thermal balance among the internal surface of the storage envelop, other envelops and the room space. Eqs. (14) denotes the impacts of solar radiance on the building envelop. Eqs. (15)–(16) represent the thermal balance between each envelop and the ambient environment. Eq. (17) represents the heat balance relationship between each wall of the building and the indoor air and other walls. In addition, Eq. (18) denotes the heat balance equation of indoor air. The heat exchange between room air and TSM and the inner wall of TSM wall

is equal to the heat exchange between the remaining walls except TSM wall and room air.

$$Q_{ctrl}^{t} + Q_{q-q}^{t} + Q_{i-q}^{t} = Q_{q-p}^{t}$$
(10)

$$Q_o^t = Q_{am-o}^t \tag{11}$$

$$Q_{o}^{t} = Q_{o-a}^{t} + Q_{o-p}^{rt} + Q_{A-o}^{t}$$
(12)

$$Q_{R-i}^{t} + \sum_{i=1}^{N} Q_{j-i}^{rt} = Q_{i-a}^{t} + Q_{i-p}^{rt} + Q_{\Delta-i}^{t}$$
(13)

$$Q_{am-k}^{rt} = \alpha_{sw} g_t \quad k = 2 \tag{14}$$

$$Q_k^t = Q_{am-k}^t + Q_{am-2}^{rt} + Q_{\Delta-k}^t \quad k = 2$$
 (15)

$$Q_k^t = Q_{am-k}^t + Q_{\Delta - k}^t \quad k \neq 2 \quad k \in \mathbb{N}$$
 (16)

$$Q_k^t = Q_{k-R}^t + \sum_{j=1, j \neq k}^{N} Q_{k-j}^t \quad k \in N$$
 (17)

$$Q_{ctrl}^{t} + Q_{R-i}^{t} = \sum_{k-1}^{N} Q_{k-R}^{t}$$
(18)

where Q_{a-p}^{\prime} , Q_{o}^{\prime} and Q_{am-o}^{\prime} are the thermal flow from the air gap to TSM, the thermal loss of the external surface and the thermal flow from ambient environment to the external surface, respectively. $Q_{\Delta-o}^{l}$, $Q_{\Delta-i}^{l}$ and $Q_{\Delta-k}^{l}$ denote the enthalpy increment of the external surface, internal surface and the envelop k, respectively. Q_{j-i}^{rl} represents the energy flow from envelop j to the internal surface. Q_{am-k}^{rl} is the thermal flow from the ambient environment to envelop j by radiation. α_{sw} is the radiation absorption coefficient. Q_k^{l} denotes the thermal loss of envelop k. Q_{k-r}^{l} and Q_{k-j}^{l} are thermal flow from envelop k to the room space and envelop j, respectively. Q_{R-j}^{l} is the thermal flow from the room space to the internal surface.

Without loss of generality, a latent heat based TSM is adopted in this paper [37]. As shown in Fig. 3(a), its specific heat capacity around the melting point is much higher than those of conventional materials, making it capable of massive energy storage with slightly core temperature change. The relationship between the specific heat capacity C_p and the core temperature T_p can be approximated by the following equation:

$$C_p(T_p) \approx \alpha T_p^2 + \beta T_p + \gamma \quad T_p^{\min} \le T_p \le T_p^{\max}$$
 (19)

where T_p^{\min} and T_p^{\max} are the lower and upper boundaries of temperature in phase change process, respectively. α , β and γ are the fitting parameters of curve in Fig. 3(a), respectively.

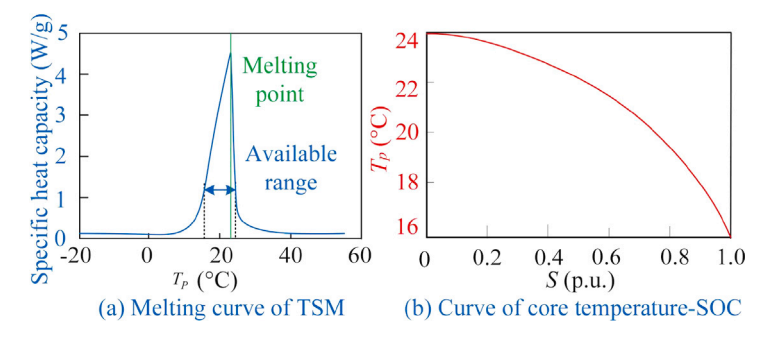


Fig. 3. The relationships between thermal and electrical variables [37].

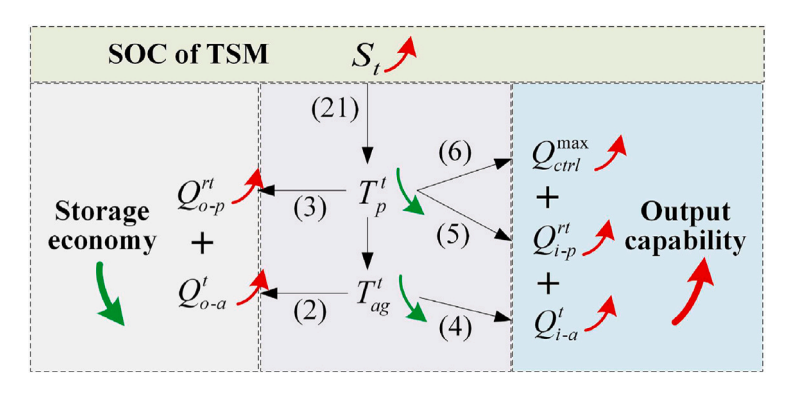


Fig. 4. Sensitive analysis of performance indexes corresponding to the variation of SOC.

When the core temperature varies from T_p^{\min} to T_p , the enthalpy difference of TSM $H\left(T_p\right)$ is formulated as:

$$H\left(T_{p}\right) = \int_{T_{p}^{\min}}^{T_{p}} m_{p} C_{p}\left(\tau\right) d\tau \tag{20}$$

where m_n is the mass of TSM.

We define the relationship between the SOC of TESS S and T_p as follows:

$$S\left(T_{p}\right) = \frac{H\left(T_{p}^{\max}\right) - H\left(T_{p}\right)}{H\left(T_{p}^{\max}\right)} \quad T_{p} \in \left[T_{p}^{\min} T_{p}^{\max}\right]$$
(21)

Substituting (19) and (20) into (21), the variable conversion equation of electrical-thermal systems can be obtained and then expressed in a compact form as Eq. (22), which is plotted in Fig. 3(b).

$$T_{p} = Y(S) \tag{22}$$

Discussion: As illustrated detailedly in Fig. 4, a higher SOC means a lower core temperature of TSM, and then a higher output capability of the thermal system. However, the increase of SOC also equals to the increment of energy loss and the deterioration of economic performance.

3. Comprehensive electrical-thermal combined robust dispatch

In this section, an electrical-thermal combined robust dispatch is formulated to deal with the coupled impacts of uncertainties on the smart building.

3.1. Electrical-thermal combined robust dispatch

We adopt the electricity market circumstances as follows: the operator of smart building participates in the energy arbitrage with day-ahead electrical purchase/sell contracts, while compensates the inter-day energy imbalance in the real-time market. This paper takes the optimal system economy under the worst scenario as the scheduling

goal, and uses the heat pump power P_{HP}^t and circulating air flow rate of the building heat storage system m_t as scheduling optimization variables to adjust the electricity-heat supply. And the feasibility of the scheduling scheme is guaranteed through relevant constraints. Specifically, the constraints include the equations and restrictions of the thermal side as (1)–(22). Constraint (23) denotes the comfort range of the temperature of room space. Constraints (24)–(27) represent the power exchange limits between the smart building and the external grid. Constraint (28) stands for the power balance in the electrical side. Equations (29)–(35) denote the correlation between the solar radiation and the PV output [38]. Constraint (36) captures the power limit of electrical—thermal conversion with HP. Eq. (37) represents the relationship between the SOC and the net thermal power. Eq. (38) denotes the influence of ambient temperature on the conversion efficiency of HP [39]. Constraint (39)–(40) are the limitations of SOC.

$$T_R^{\min} \le T_R^t \le T_R^{\max} \quad \forall t \tag{23}$$

$$0 \le P_{db}^t, P_{ds}^t \le P_d^{\text{max}} \quad \forall t \tag{24}$$

$$0 \le P_{rb}^t, P_{rs}^t \le P_r^{\max} \quad \forall t \tag{25}$$

$$P_{dh}^t + P_{rh}^t \le P_L^{\text{max}} \quad \forall t \tag{26}$$

$$P_{ds}^t + P_{rs}^t \le P_L^{\max} \quad \forall t \tag{27}$$

$$P_{db}^{t} - P_{ds}^{t} + P_{rb}^{t} - P_{rs}^{t} + P_{PV}^{t} - P_{L}^{t} - P_{HP}^{t} = 0$$
(28)

$$P_{PV}^{t} = \frac{\eta_e^t P_{STC}}{\eta_0 G_{STC}} g_t \quad \forall t$$
 (29)

$$\eta_e^t = \eta_0 \left[1 - \beta \left(T_{PV}^t - T_0 \right) \right] \quad \forall t \tag{30}$$

$$E_c^t = p\alpha_c \tau_g g_t \tag{31}$$

$$E_{ce}^t = p \eta_e^t \tau_g g_t \tag{32}$$

$$E_{ct}^t = E_c^t - E_{ce}^t \tag{33}$$

$$E_T^t = (1 - p) \alpha_T \tau_\sigma g_t \tag{34}$$

$$E_{ct}^t + E_T^t = 2 \cdot h_{PV} A_{PV} \left(T_{PV}^t - T_{am}^t \right) \quad \forall t \tag{35}$$

$$0 \le P_{HP}^t \le P_{HP}^{\max} \quad \forall t \tag{36}$$

$$S_{t} = S_{t-1} + \frac{\mu_{t} P_{HP}^{t} - P_{HL}^{t}}{H \left(T_{D}^{\text{max}}\right)} \quad \forall t$$
 (37)

$$\mu_t = -0.14 \left(T_{am}^t - 35 \right) + \mu_0 \tag{38}$$

$$S_t \ge 0 \quad \forall t \tag{39}$$

$$S_{N_T} \ge S_0 \tag{40}$$

where p_{db}^t , p_{ds}^t , p_{rb}^t and p_{rs}^t are the day-ahead purchase and day-ahead sell, real-time purchase and real-time sell price, respectively. P_{db}^{t} , P_{ds}^{t} , P_{rb}^{t} , P_{rs}^{t} stand for the day-ahead purchase, day-ahead sell, real-time purchase and real-time sell power, respectively. T_R^{\min} and T_R^{\max} denote the comfort range. P_d^{\max} , P_r^{\max} and P_L^{\max} are the upper limit of the power exchange. P_{PV}^t , P_L^t and P_{HP}^t represent the power of PV, conventional loads and HP, respectively. η_e^t , η_0 , β are the coefficients of PV thermal process. T_{PV}^t and T_0 are the real-time and ideal temperature, respectively. E_c^t , E_{ce}^t and E_{ct}^t are the total energy absorbed, the electrical energy produced and the thermal energy released, respectively. E_T^t is the solar energy absorbed by the back-sheet of PV cell. h_{PV} and A_{PV} represent the convective coefficient and the contact area between the back-sheet and the front of PV panel, respectively. μ_t and μ_0 are the real-time coefficient of performance (COP) and ideal COP of HP, respectively.

Combining (29)-(35), we obtain the nonlinear equation including PV efficiency, solar radiation and ambient temperature.

$$\begin{split} P_{PV} &= \varpi\left(g, T_{am}\right) = \frac{P_{STC}}{G_{STC}} \cdot g \cdot \\ &\left[p a_c + (1 - p) a_T\right] \beta \tau_g g - 2 \cdot h_{PV} A_{PV} \left[1 + \beta \left(T_0 - T_{am}\right)\right] \\ &p \beta \tau_g \eta_0 g - 2 \cdot h_{PV} A_{PV} \end{split} \tag{41}$$

To deal with the nonlinearity in Eq. (41), the first order Taylor series method is adopted as follows. By this means, the PV output (29)-(35) can be approximated and replaced by Eqs. (42)-(43).

$$k_{PV}^{t} = \left. \frac{\partial \varpi \left(g, T_{am} \right)}{\partial g} \right| g = \tilde{g}_{t}, T_{am} = T_{am}^{t}$$
(42)

$$P_{PV}^{t} = k_{PV}^{t} \left(g - \tilde{g} \right) + \varpi \left(\tilde{g}, T_{am}^{t} \right) \tag{43}$$

3.2. Uncertainty set of environmental factors

It can be seen from Section 3.A that the thermal side and the electrical side are mainly impacted by the uncertainty of solar radiation. Therefore, we adopt it as the uncertainty factor in this paper.

$$G = \begin{cases} g & g_t = \tilde{g}_t + g_t^+ - g_t^-, & 0 \le g_t^+ \le z_t^+ \hat{g}_t^+ \\ 0 \le g_t^- \le z_t^- \hat{g}_t^-, & (z_t^+, z_t^-) \in \{0, 1\} \\ z_t^+ + z_t^- \le 1, & \sum_{t=1}^{N_T} \frac{g_t^+ + g_t^-}{\tilde{g}_t} \le \Gamma \end{cases}$$

$$(44)$$

where \tilde{g}_t , g_t^+ and g_t^- are the predicted nominal value, upward bias and downward bias of the solar radiation, respectively. \hat{g}_t^+ and \hat{g}_t^- are the upper bound and lower bound, respectively. z_t^+ and z_t^- are mutually exclusive variables. Γ is the budget of uncertainty.

3.3. Compact model

For notation brevity, we use matrices and vectors to represent the constraints and variables in a compact form as follows. Constraint (46) denotes (1)-(5), (8), (10)-(18). Constraint (47) represents (19)-(22). Constraint (48) stands for (23). Constraint (49) represents (7). Constraint (50) denotes (24)-(27). Constraint (51) denotes (28), (42) and (43). Constraint (52) stands for (36)-(38). Constraint (53) represents (39)-(40).

$$\min_{x,s} \mathbf{c}^{\mathrm{T}} x + \max_{g \in G} \min_{y,z,m} \mathbf{d}^{\mathrm{T}} y \tag{45}$$

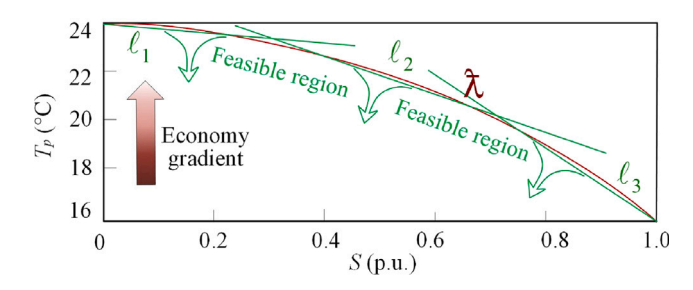


Fig. 5. Piecewise linearization of the temperature-SOC curve.

$$Cz+Dg+Ec+Fm+Icm=a$$
(46)

$$\mathbf{J}c + \mathbf{K}Y(s) = 0 \tag{47}$$

$$\mathbf{H}z \ge \mathbf{f} \tag{48}$$

$$Gm \ge b \tag{49}$$

$$\mathbf{X}x + \mathbf{Y}y \ge \mathbf{p} \tag{50}$$

$$\mathbf{N}x + \mathbf{P}y + \mathbf{Q}g \ge \mathbf{q} \tag{51}$$

$$\mathbf{R}s + \mathbf{N}x + \mathbf{P}y + \mathbf{W}z + \mathbf{Q}g + \mathbf{Y}c + \mathbf{V}m + \mathbf{J}cm = \mathbf{r}$$

$$\mathbf{Z}s \ge \mathbf{j}$$
(52)

where
$$\mathbf{v} = [P^t \quad P^t \mid T]^T$$
 $\mathbf{v} = [P^t \quad P^t \mid T]^T$ $\mathbf{v} = [S \mid T]^T$ $\mathbf{m} = [m]^T$

where
$$x = [P_{db}^t, P_{ds}^t]^T$$
, $y = [P_{rb}^t, P_{rs}^t]^T$, $s = [S_t]^T$, $m = [m_t]^T$, $z = [T_o^t, T_{ag}^t, T_t^t, T_R^t, T_t^t, T_2^t, T_3^t]^T$, $c = [T_p]^T$.

4. Solution algorithm

4.1. Piecewise linearization of electrical-thermal conversion equations

In this subsection, we will try to replace the nonlinear Eq. (47) with linear ones. We assume that there is a feasible region formulated by linear constraints l_1 , l_2 , l_3 , and presented in a compact form as (54).

$$\mathbf{A}c + \mathbf{B}s \le \mathbf{h} \tag{54}$$

As shown in Fig. 5, the same SOC corresponds to various T_n , which means that (54) is not equal to Eq. (47) from a mathematical perspective. However, according to the discussion in Section 2.B, the higher of T_n , the better economic performance of TES. On account that objective (45) aims to minimize the total cost, T_p will always reach the upper boundary of the feasible region in the optimization process. Therefore, (47) can be approximated by (54).

However, the thermal side control may be infeasible due to its possible low-SOC status. Under this circumstance, (47) and (54) will no longer be equivalent. To deal with problem, an additional constraint is needed to ensure that there is at least one feasible solution for controllable variable m with any $g \in G$.

Let the mass flow $m_t = m^{\text{max}}$ to maximize the thermal output capability, we try to find the upper boundary of TSM temperature to guarantee the feasibility of the indoor temperature regulation.

$$\Re = \max_{c,z} c_{ub} \tag{55}$$

 $c_{ub} \leq c$

Cz+Dg+Ec+Fm+Icm = a

 $Hz \ge f$

 $\forall g \in G$

With the conversion equation, the optimized result can be transformed into the lower boundary limit of SOC and denoted as an additional constraint by modifying constraint (53).

$$s \ge Y^{-1}\left(c_{ub}\right) \tag{56}$$

4.2. Decomposition algorithm of RO

We denote $\bar{\theta}$ as the second-stage optimal economic dispatch cost under the worst case scenario. Then the master problem can be described as follows.

$$\Gamma = \min_{x,c,s} \mathbf{c}^{\mathrm{T}} x + \bar{\theta} \tag{57}$$

(53)-(54)

Feasibility cuts

Optimality cuts

The second-stage optimal economic dispatch can be formulated as a max-min problem.

$$\Pi = \max_{g \in G} \min_{y, z, m} d^{\mathrm{T}} y$$
s.t.
(58)

$$\begin{aligned} \mathbf{C}z + \mathbf{F}m + \mathbf{I}\hat{c}m &= \mathbf{a} - \mathbf{D}g - \mathbf{E}\hat{c} &\rightarrow \alpha \\ \mathbf{H}z &\geq \mathbf{f} &\rightarrow \beta \\ \mathbf{G}m &\geq \mathbf{b} &\rightarrow \chi \\ \mathbf{Y}y &\geq \mathbf{p} - \mathbf{X}\hat{x} &\rightarrow \varepsilon \\ \mathbf{P}y &\geq \mathbf{q} - \mathbf{N}\hat{x} - \mathbf{Q}g &\rightarrow \phi \\ \mathbf{P}y + \mathbf{V}m + \mathbf{J}\hat{c}m + \mathbf{W}z &= r - \mathbf{R}\hat{s} - \mathbf{N}\hat{x} - \mathbf{Q}g - \mathbf{Y}\hat{c} \rightarrow \varphi \end{aligned}$$

Based on the strong duality theory, the second-stage max–min problem Π can be transformed into a max problem. Nevertheless, the objective function of the dual formulation contains the multiple of g with the dual variables α , ϕ and φ . We apply the bilinear approach by decomposing the dual formulation into two linear slave problems.

$$\begin{split} \boldsymbol{\Pi}_{1}\left(x,c,s,g\right) &= \max_{\boldsymbol{\alpha},\boldsymbol{\beta},\boldsymbol{\chi},\boldsymbol{\epsilon},\boldsymbol{\phi},\boldsymbol{\varphi}} \left(\mathbf{a} - \mathbf{D}g - \mathbf{E}\hat{c}\right)^{T}\boldsymbol{\alpha} \\ &+ \mathbf{f}^{T}\boldsymbol{\beta} + \mathbf{b}^{T}\boldsymbol{\chi} + \left(\mathbf{p} - \mathbf{X}\hat{x}\right)^{T}\boldsymbol{\epsilon} + \left(\mathbf{q} - \mathbf{N}\hat{x} - \mathbf{Q}g\right)^{T}\boldsymbol{\phi} \\ &+ \left(\mathbf{r} - \mathbf{R}\hat{s} - \mathbf{N}\hat{x} - \mathbf{Q}g - \mathbf{Y}\hat{c}\right)^{T}\boldsymbol{\varphi} \end{split}$$

s.t.

 $\begin{aligned} \mathbf{Y} \varepsilon + \mathbf{P} \phi + \mathbf{P} \varphi &\leq \mathbf{d} \\ (\mathbf{F} + \mathbf{I} \hat{c}) \, \alpha + \mathbf{G} \chi + (\mathbf{V} + \mathbf{J} \hat{c}) \, \varphi &\leq 0 \end{aligned}$

 $\mathbf{C}\alpha + \mathbf{H}\beta + \mathbf{W}\varphi \le 0$ $\beta, \chi, \varepsilon, \phi \ge 0$

and

$$\begin{split} \boldsymbol{\varPi}_2\left(\boldsymbol{x}, \boldsymbol{c}, \boldsymbol{s}, \boldsymbol{\alpha}, \boldsymbol{\beta}, \boldsymbol{\chi}, \boldsymbol{\varepsilon}, \boldsymbol{\phi}, \boldsymbol{\varphi}\right) &= \max_{\boldsymbol{g} \in G} \left(-\boldsymbol{\alpha}^T \mathbf{D} - \boldsymbol{\phi}^T \mathbf{Q} - \boldsymbol{\varphi}^T \mathbf{Q} \right) \boldsymbol{g} \\ &+ \boldsymbol{\alpha}^T \mathbf{a} - \boldsymbol{\alpha}^T \mathbf{E} \hat{\boldsymbol{c}} + \mathbf{f}^T \boldsymbol{\beta} + \mathbf{b}^T \boldsymbol{\chi} + (\mathbf{p} - \mathbf{X} \hat{\boldsymbol{x}})^T \boldsymbol{\varepsilon} \\ &+ \boldsymbol{\phi}^T \left(\mathbf{q} - \mathbf{N} \hat{\boldsymbol{x}} \right) + \boldsymbol{\varphi}^T \left(\mathbf{r} - \mathbf{R} \hat{\boldsymbol{s}} - \mathbf{N} \hat{\boldsymbol{x}} \right) \end{split}$$

Note that Π_2 is feasible and bounded from above because the feasible region of $g \in G$ is a polyhedral, and the objective function is continuous. Therefore, we merely need to check the feasibility of Π_1 by constructing a series of non-auxiliary variables to generate feasibility cuts with the L-shaped method, which is detailedly illustrated in Ref. [33].

The detailed solution procedures are illustrated as follows.

- (1) Solve reliability subproblem \Re , and add the reliability cut $s \ge s_{lb}$ to master problem Γ .
- (2) Solve master problem Γ, and store its optimized variables x, s, and c.
- (3) Check the feasibility of Π_1 . If feasible, go to Step (4), otherwise, add a feasibility cut to master problem Γ , and go to Step (2).
- (4) Solve slave problems Π_1 and Π_2 iteratively, and save the optimized objective $\Pi_1(x,c,s,g)$.

(5) If $\Pi_1(x,c,s,g) > \bar{\theta}$, add the corresponding optimality cut $\Pi_1(x,c,s,g) \leq \bar{\theta}$ to the master problem. Otherwise, terminate the optimization and output the scheduling scheme.

For the above model, this paper writes a program on the MATLAB platform and uses Yalmip to call the CPLEX solver for solution.

5. Numerical analysis

We assume that there is a smart building with 1500 kW rooftop PV and 400 rooms. The room size is 4500*4500* 3000 mm. Each room is equipped with a TES unit with 600 kg TSM, a HP with 3 kW rated power and a circulating fan with a maximum airflow rate m_{\star}^{max} of 5 kg/s. The detailed thermal parameters can be found in Ref. [37]. Based on the neural network, the classic meteorological data of Shenzhen, China are analyzed, and the predicted curves of ambient temperature and solar radiation are illustrated in Fig. 6. According to the prediction accuracy of solar radiation intensity by existing technologies, the random fluctuation in this paper selects the truncated normal distribution with a fluctuation within $\pm 20\%$ around the predicted value under the most conservative condition. The curves of conventional loads and day-ahead purchase electricity price are shown in Fig. 7. The day-ahead sell price, real-time purchase price and real-time sell price are -0.1 CNY/kWh, +0.2 CNY/kWh and -0.2 CNY/kWh compared with the day-ahead purchase price, and the comfort range is set to be $20\,^{\circ}\text{C} \sim 25\,^{\circ}\text{C}$.

5.1. Thermodynamic analysis of smart building

In this section, we analyze the thermal performance of the smart building corresponding to various SOC and the ambient environment. Set m_t to be the maximum, and the SOC ranges from 1% to 100%. To maintain the uniformity, the thermal power in this section will be converted into electrical power with the ideal COP of HP. As shown in Fig. 8, the thermal output capability increases with the increase of SOC. Take the cases in 12:00 for instance, the output capability with 100% SOC is 612 kW, but the one with 10% SOC is 326 kW, only taking up 53.3% of the peak value. Besides, the capability will also be effected by the ambient environment that, with 50% SOC, the output capability is 317 kW in 8:00, which is the valley hour for the ambient temperature and solar radiation. In contrast, the peak output capability is 626 kW in 15:00.

As illustrated in Fig. 9, a higher SOC means a higher heat leakage of the smart building. More specifically, the heat leakage in 12:00 with 100% SOC is 62 kW, 1.86 times to the one with 10% SOC. The results above indicate the heat leakage is an expense for a better thermal performance, and a trade-off should be considered in the scheduling to balance the heat storage loss and the output capability.

The impacts of solar uncertainties on PV generation and heat demand are presented in Fig. 10. In these cases, the objective of thermal side control is set to minimize the thermal demand. Fig. 10 shows that the maximum fluctuation range of the PV power is 198 kW, while the one of the thermal demand is 32 kW. It can be seen that, the impacts on the thermal side reach 16.2% of the one on electrical side. The case study verifies that the uncertainty of solar radiation has coupled impacts on the electrical system and the thermal system.

5.2. Performance analysis of dispatch approach

In this subsection, the performance of the proposed approach is evaluated, compared with other schemes. Scheme 1 is a deterministic dispatch regarding the thermal system as an ideal controllable load. Scheme 2 stands for a deterministic dispatch which considers the operation details of thermal systems such as thermal output capability and heat storage loss. Scheme 3 considers the impacts of uncertainties on the thermal side independently and then takes the worst thermal

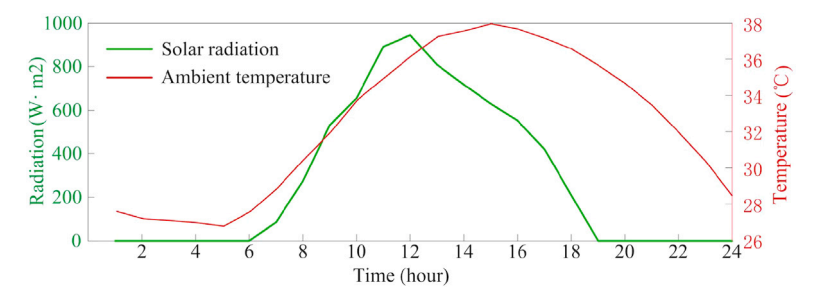


Fig. 6. Day-ahead prediction of ambient temperature and solar radiation.



Fig. 7. Conventional loads and day-ahead purchase price.

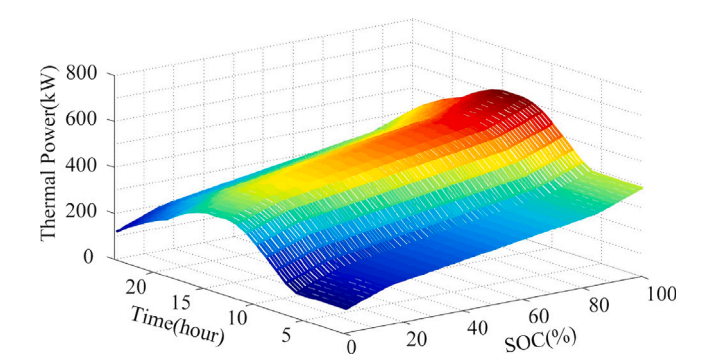


Fig. 8. Thermal output capability with various SOC and ambient environment.

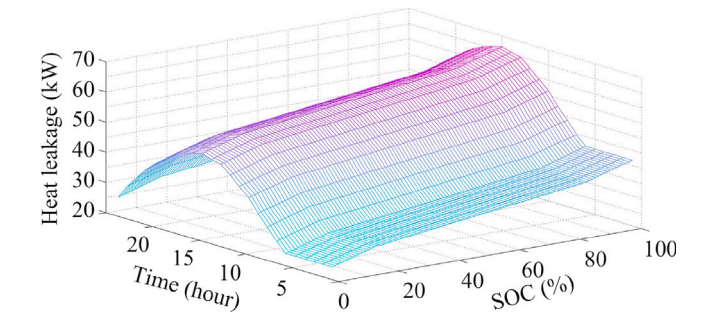


Fig. 9. Heat storage leakage with various SOC and ambient environment.

case into account in the electrical side robust dispatch. Scheme 4 is the approach proposed in our work.

The related values of day-ahead electricity purchase/sale contract of the above schemes are shown in Fig. 11. We can observe that the electricity purchasing behavior in Scheme 1 mainly occurs at the valley hours with the lowest price. Nevertheless, Schemes 2, 3 and 4, which consider the factor of heat storage loss as well, schedule their electricity purchase hours much closer to the period with higher heat consumptions, despite the prices in these hours are not the lowest. In addition,

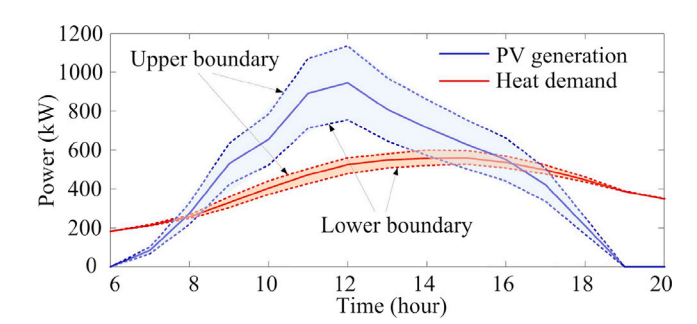


Fig. 10. Impacts of the uncertainty of solar radiation on electrical and thermal systems.

the energy purchased in the day-ahead stage of the four schemes are 6228 kWh, 6452 kWh, 7266 kWh, and 6879 kWh, respectively. It can be seen that, the purchased energy of robust dispatch schemes is more substantial than that of the deterministic ones. Meanwhile, by comprehensively considering the impacts of uncertainty, Scheme 4 purchases less energy than that of Scheme 3 which considers the thermal side and electrical side impacts independently, indicating that the electrical-thermal combined approach ameliorates the conservativeness of robust dispatch for the smart building.

The real-time purchase/sell activities of the smart building are demonstrated in Fig. 12. We assume that the day-ahead forecast is accurate. Under the condition, Scheme 1 has unexpected purchasing and selling behavior because of the over-idealized thermal model, Scheme 2 has just reached its expected working profile, while Scheme 3 and Scheme 4 sell the over-bought energy 978 kWh and 631 kWh to the external power grid, respectively. The discrepancies between Scheme 1 and Scheme 2 further verify that the ideal thermodynamic model cannot adequately reflect the real operation of the thermal system. Compared with Schemes 1 and 2, Schemes 3 and 4 buy more electricity at the day-ahead stage while sell more at the real-time one, leading to the deterioration of economic performance. Compared with Scheme 4, Scheme 3 interacts deeper with the external grid, indicating that it has made a more conservative estimation for the worst case.

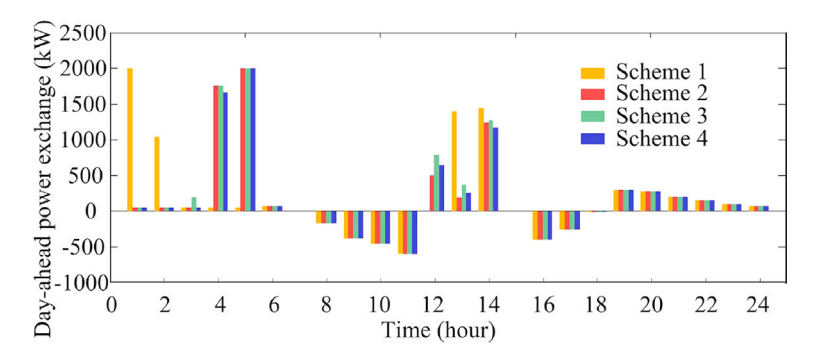


Fig. 11. Day-ahead purchase/sell activities of the smart building.

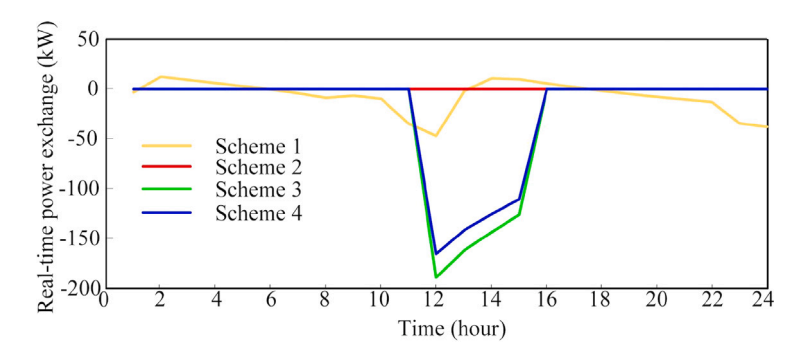


Fig. 12. Real-time purchase/sell activities of the smart building.

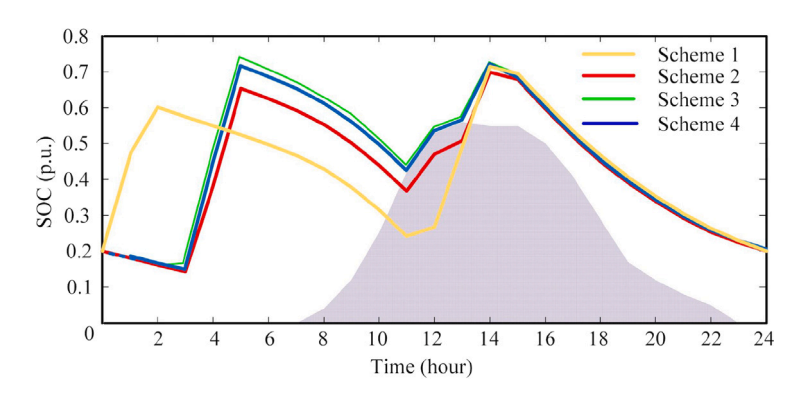


Fig. 13. SOC scheduled in the day-ahead stage.

The solid colored lines in Fig. 13 denote the SOC of each scheme, and the shadow area defines the lower boundary of SOC based on Eq. (56). It can be seen that Schemes 3 and 4 can always keep their SOC above the boundary, while the SOC curves of Schemes 1 and 2 will enter the shadow area during 11:00–14:00, thus bring about infeasible risks to the thermal control. To verify the effectiveness of lower boundary of SOC, we generate 200 cases with random solar radiation to check the feasibility of thermal control, and the indoor temperature curves are recorded in Fig. 14. The result shows that all the temperature curves of Scheme 1 violate the indoor comfort limit, while only parts of the cases in Scheme 2 are infeasible. In contrast, Schemes 3 and 4, which are precautionary against the thermal side impacts, are feasible in all random cases, which further confirms the significance of considering the impacts of uncertainty on the thermal side. The results of scheme 2 to 4 are compared in Table 2.

As we can see, the reliability restrictions are only well met by Schemes 3 and 4. Therefore, we merely evaluate the economic performance for those two schemes with different budget of uncertainty $\Gamma(0.05, 0.10, 0.15 \text{ and } 0.20)$. According to Fig. 15, with the increase of

 Γ , the upper boundary of the operation cost continues to decline that the cost of Scheme 3 decreases from 2693 CNY to 2588 CNY, while the cost of Scheme 4 decreases from 2658 CNY to 2516 CNY, by a decline of 3.9% and 5.3%, respectively. Meanwhile, the mean value of the cost of Schemes 3 and 4 rise by 2.4% and 1.3%, respectively. The above results indicate that, on the one hand, the choice of budget of uncertainty will make a tradeoff between the maximum cost and the average cost. On the other hand, the economic performance of Scheme 4 is superior to that of Scheme 3 which considers power system and thermal system independently, proving that by considering the impacts of uncertainty comprehensively, the proposed dispatch could eliminate unlike-to-happen scenarios and further limit the level of conservatism of the robust solution.

6. Conclusion

In this paper, we formulate a comprehensive modeling framework that jointly considers the simultaneous impacts of environmental uncertainties on the thermal systems and electrical systems. The case studies show the following conclusions:

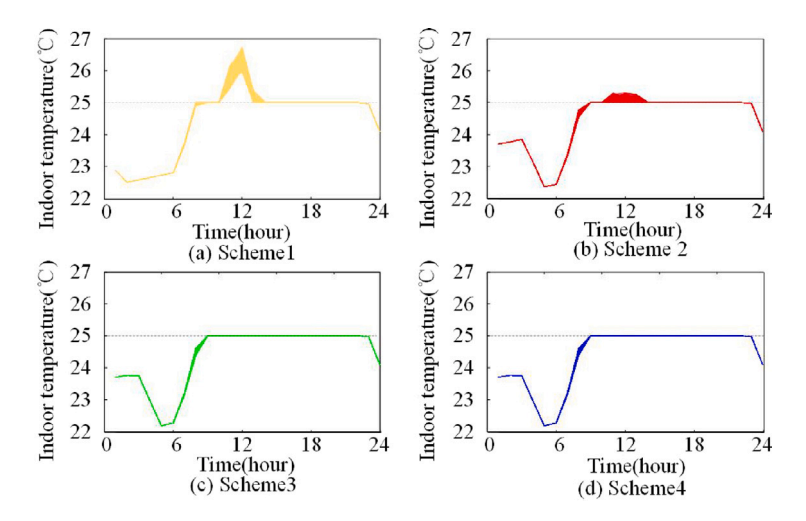


Fig. 14. Indoor temperature of various dispatch schemes.

Table 2
Results of scheme 2 to 4.

Scheme	day-ahead purchase (kWh)	real-time sell (kWh)	Room temperature control	Maximum cost(CNY)
2	6452	0	Out of control	2446
3	7266	959	Controllable	2588
4	6879	601	Controllable	2516

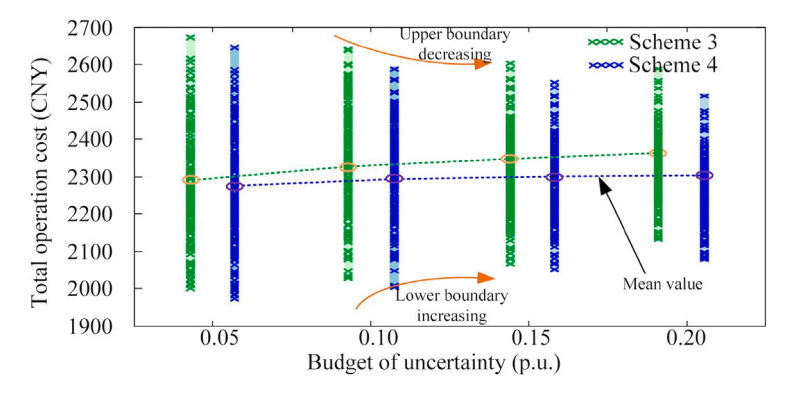


Fig. 15. The operation cost distribution of smart building under different Γ .

- (1) Compared with the ideal thermodynamic model, the refined thermal network model proposed in this paper can reflect the actual operation of the thermal system and is more applicable. Meanwhile, the uncertainty of solar radiation affects both photovoltaic power generation output and building thermal demand. Moreover, the impact of solar radiation uncertainty on the thermal side accounts for 16.2% of the impact on the electrical side, which cannot be ignored.
- (2) Compared to deterministic optimization scheduling models, the proposed electricity—thermal joint robust optimization scheduling model takes into account uncertainties on both the electrical and thermal sides, with the results of room temperature control being robust. At the same time, compared to robust optimization method that only considers the uncertainty on the thermal side independently and does not couple the electric and thermal sides, the electricity-thermal joint robust optimization scheduling model can accurately assess the worst-case scenario and reduce average costs by 4.2% (Γ =0.20) while ensuring the reliability of the energy supply.
- (3) As the uncertainty increases from 0.05 to 0.20, the worst-case maximum daily operating cost decreases by 4.6% and the average daily operating cost increases by 1.5%. The dispatcher can

flexibly adjust the uncertainty parameter Γ in the robust optimization model to make a trade-off between the conservatism and economy of the strategy.

CRediT authorship contribution statement

Weijie He: Writing – original draft, Conceptualization. Fanrong Wei: Data curation. Xiangning Lin: Funding acquisition. Samir M. Dawoud: Software.

Declaration of competing interest

The authors declare that they have no known competing financial interests or personal relationships that could have appeared to influence the work reported in this paper.

Acknowledgments

This work was supported by the National Nature Science Foundation of China (Grant number U22B20106) and the National Key Research and Development Program of China (Grant number 2022YFE0120400).

Data availability

Data will be made available on request.

References

- [1] Yue L, Niu J, Tian Z, Lin Q, Lu Y. A comprehensive evaluation framework for building energy systems considering economic efficiency, independence, and building-grid interaction performance indicators. Energy Build 2024;318:114414.
- [2] Kumar M. Control techniques for operation of roof-top solar photovoltaics based microgrid in islanded mode. Int J Electr Power Energy Syst 2024;155:109511.
- [3] Chegari B, Tabaa M, Simeu E, El Ganaoui M. Optimal energy management of a hybrid system composed of PV, wind turbine, pumped hydropower storage, and battery storage to achieve a complete energy self-sufficiency in residential buildings. IEEE Access 2024;12:126624–39.
- [4] Zhao G, Clarke J, Searle J, Lewis R, Baker J. Economic analysis of integrating photovoltaics and battery energy storage system in an office building. Energy Build 2023;284:112885.
- [5] Moulakhnif K, Ait Ousaleh H, Sair S, Bouhaj Y, El Majd A, Ghazoui M, et al. Renewable approaches to building heat: exploring cutting-edge innovations in thermochemical energy storage for building heating. Energy Build 2024:318:114421.
- [6] Meng Y, Tan Y, Li X, Cai Y, Peng J, Long Y. Building-integrated photovoltaic smart window with energy generation and conservation. Appl Energy 2022:324:119676.
- [7] Sun J, Zhao J, Zhang W, Xu J, Wang B, Wang X, et al. Composites with a novel core-shell structural expanded perlite/polyethylene glycol composite PCM as novel green energy storage composites for building energy conservation. Appl Energy 2023;330:120363.
- [8] Qiu G, Li K, Cai W, Yu S. Optimization of an integrated system including a photovoltaic/thermal system and a ground source heat pump system for building energy supply in cold areas. Appl Energy 2023;349:121698.
- [9] Jiang T, Li Z, Jin X, Chen H, Li X, Mu Y. Flexible operation of active distribution network using integrated smart buildings with heating, ventilation and air-conditioning systems. Appl Energy 2018;226:181–96.
- [10] Lizana J, Friedrich D, Renaldi R, Chacartegui R. Energy flexible building through smart demand-side management and latent heat storage. Appl Energy 2018;230:471–85.
- [11] Wang L, Guo L, Ren J, Kong X. Using of heat thermal storage of PCM and solar energy for distributed clean building heating: A multi-level scale-up research. Appl Energy 2022;321:119345.
- [12] Azad A, Shateri H. Design and optimization of an entirely hybrid renewable energy system (WT/PV/BW/HS/TES/EVPL) to supply electrical and thermal loads with considering uncertainties in generation and consumption. Appl Energy 2023;336:120782
- [13] Violante W, Cañizares CA, Trovato MA, Forte G. An energy management system for isolated microgrids with thermal energy resources. IEEE Trans Smart Grid 2020;11(4):2880-91.
- [14] Rostamnezhad Z, Mary N, Dessaint L-A, Monfet D. Electricity consumption optimization using thermal and battery energy storage systems in buildings. IEEE Trans Smart Grid 2023;14(1):251–65.
- [15] Zhang L, Feng G, Huang K, Bi Y, Chang S, Li A. Design and optimization for photovoltaic heat pump system integrating thermal energy storage and battery energy storage. Energy Build 2025;329:115277.
- [16] Li D, Zhang Z, Feng D, Zhou Y, Bai X, Zhao J. Multi-objective two-stage robust optimization of wind/PV/thermal power system based on meta multi-agent reinforcement learning. Int J Electr Power Energy Syst 2024;162:110273.
- [17] Wei F, Li Y, Sui Q, Lin X, Chen L, Chen Z, et al. A novel thermal energy storage system in smart building based on phase change material. IEEE Trans Smart Grid 2019;10(3):2846–57.

- [18] Dai Y, Chen L, Min Y, Mancarella P, Chen Q, Hao J, et al. Integrated dispatch model for combined heat and power plant with phase-change thermal energy storage considering heat transfer process. IEEE Trans Sustain Energy 2018;9(3):1234–43.
- [19] Tan J, Wu Q, Zhang X. Optimal planning of integrated electricity and heat system considering seasonal and short-term thermal energy storage. IEEE Trans Smart Grid 2023;14(4):2697–708.
- [20] Sharma S, Verma A, Xu Y, Panigrahi BK. Robustly coordinated bi-level energy management of a multi-energy building under multiple uncertainties. IEEE Trans Sustain Energy 2021;12(1):3–13.
- [21] Liu X, Xu X, Wu Q, Chen X, Wen J, Wang W, et al. Soc threshold optimization for battery storage in frequency regulation considering uncertainty of SoC measurement and automatic generation control fatigue loss of thermal power system. Int J Electr Power Energy Syst 2022;137:107771.
- [22] Li Z, Xu Y, Wang P, Xiao G. Coordinated preparation and recovery of a postdisaster multi-energy distribution system considering thermal inertia and diverse uncertainties. Appl Energy 2023;336:120736.
- [23] Zhou H, Li Z, Zheng JH, Wu QH, Zhang H. Robust scheduling of integrated electricity and heating system hedging heating network uncertainties. IEEE Trans Smart Grid 2020;11(2):1543–55.
- [24] Chen S, Wei Z, Sun G, Cheung KW, Wang D, Zang H. Adaptive robust day-ahead dispatch for urban energy systems. IEEE Trans Ind Electron 2019;66(2):1379–90.
- [25] Tan M, Liu Y, Wang S, Peng F, Wang A, Zhou B. Effect of step-change of solar radiation on human thermal response under non-air-conditioned environments in winter: A field study. Energy Build 2024;321:114641.
- [26] Yaman K, Arslan G. The impact of hourly solar radiation model on building energy analysis in different climatic regions of Turkey. Build Simu 2018;11(3):483–95.
- [27] Chen JP, Dong HR. Influence of solar radiation of external decorative materials on heat consumption of buildings. Adv Mater Res 2012;512–515:2758–61.
- [28] Thang V, Ha T, Li Q, Zhang Y. Stochastic optimization in multi-energy hub system operation considering solar energy resource and demand response. Int J Electr Power Energy Syst 2022;141:108132.
- [29] Dehghani NL, Shafieezadeh A. Multi-stage resilience management of smart power distribution systems: A stochastic robust optimization model. IEEE Trans Smart Grid 2022;13(5):3452–67.
- [30] Papavasiliou A, Mou Y, Cambier L, Scieur D. Application of stochastic dual dynamic programming to the real-time dispatch of storage under renewable supply uncertainty. IEEE Trans Sustain Energy 2018;9(2):547–58.
- [31] Wang F, Zhou L, Ren H, Liu X, Talari S, Shafie-khah M, et al. Multi-objective optimization model of source-load-storage synergetic dispatch for a building energy management system based on TOU price demand response. IEEE Trans Ind Appl 2018;54(2):1017–28.
- [32] Li Z, Xu Y, Fang S, Zheng X, Feng X. Robust coordination of a hybrid AC/DC multi-energy ship microgrid with flexible voyage and thermal loads. IEEE Trans Smart Grid 2020;11(4):2782–93.
- [33] Zou Y, Xu Y, Li J. Aggregator-network coordinated peer-to-peer multi-energy trading via adaptive robust stochastic optimization. IEEE Trans Power Syst 2024.
- [34] Sun X, Cao X, Zeng B, Zhai Q, Başar T, Guan X. Stochastic-robust planning of networked hydrogen-electrical microgrids: A study on induced refueling demand. IEEE Trans Smart Grid 2025;16(1):115–30.
- [35] Peng C, Xie P, Pan L, Yu R. Flexible robust optimization dispatch for hybrid wind/photovoltaic/hydro/thermal power system. IEEE Trans Smart Grid 2016;7(2):751-62.
- [36] Wei F, Li Y, Sui Q, Lin X, Chen L, Chen Z, et al. A novel thermal energy storage system in smart building based on phase change material. IEEE Trans Smart Grid 2018, 1–1.
- [37] Lamberg P, Lehtiniemi R, Henell A-M. Numerical and experimental investigation of melting and freezing processes in phase change material storage. Int J Therm Sci 2004;43(3):277–87.
- [38] Teo H, Lee P, Hawlader M. An active cooling system for photovoltaic modules. Appl Energy 2012;90(1):309–15.
- [39] Mahdavi N, Braslavsky JH, Perfumo C. Mapping the effect of ambient temperature on the power demand of populations of air conditioners. IEEE Trans Smart Grid 2018;9(3):1540–50.